Microstructures

Research Article

K$_6$Sn$_4$F$_{12}$I$_2$•0.5H$_2$O: a zero-dimensional alkali metal tin mixed halide compound exhibiting color change due to crystal water loss

Pifu Gong[1], Siyang Luo[1], Zheshuai Lin[1,2]

[1]Chinese Academy of Sciences, Technology, Technical Institute of Physics and Chemistry, Beijing 100190, China.
[2]University of Chinese Academy of Sciences, Center of Materials Science and Optoelectronics Engineering, Beijing 100049, China.

Correspondence to: Prof. Zheshuai Lin, Chinese Academy of Sciences, Technology, Technical Institute of Physics and Chemistry, 29, Zhong Guan Cun East Road, Beijing 100190, China. E-mail: zslin@mail.ipc.ac.cn

Abstract

A new zero-dimensional alkali-metal tin mixed halide, K$_6$Sn$_4$F$_{12}$I$_2$•0.5H$_2$O, is synthesized by a hydrothermal method. It crystallizes in the cubic centrosymmetric space group of Fd-3m (No. 227) and its structure consists of crystal water molecules and ordered arranged [Sn$_4$F$_{12}$I$_4$] fundamental structural blocks trapped in [K$_{18}$] cages. Interestingly, K$_6$Sn$_4$F$_{12}$I$_2$•0.5H$_2$O exhibits a color change from colorless to orange when exposed to air. Experimental measurements combined with theoretical calculations reveal that the color change in K$_6$Sn$_4$F$_{12}$I$_2$•0.5H$_2$O is attributed to the loss of crystal water.

Keywords: Metal halide, color change, new material exploration

INTRODUCTION

Metal halides have been researched in detail as a result of their structural and functional diversity, which has resulted in many important and interesting optoelectronic applications, such as photovoltaics, photoelectricity, nonlinear optics and photoluminescence[1-11]. According to the structure-property relationship, these optoelectronic properties are determined by their microstructures. For example, by

reducing the structural dimensions from three dimensions to zero dimensions to promote the recombination of photogenerated carriers, $(TTA)_2SbCl_5$ and $(bmpy)_9[ZnCl_4]_2[Pb_3Cl_{11}]$ have realized ultrahigh photoluminescence quantum yield[12,13]. Moreover, through halogen element hybridization, metal halides, such as $Cs_2HgI_2Cl_2$, $Rb_2CdBr_2I_2$ and $K_2SbF_2Cl_3$, $[NH_2(CH_2CH_3)_2]_3Bi(Cl_{1-x}Br_x)_6$, have significantly improved the laser damaged threshold and can maintain their nonlinear optical effects simultaneously, which make them good candidates as nonlinear optical materials in the infrared spectral region[14-17]. Considering their excellent optoelectronic properties and important applications, it is necessary to continue the research of structure-property relationships in metal halides.

Metal halides are normally obtained by solution or hydrothermal methods, where water can play an important role in determining their structures and optoelectronic properties. For example, by introducing water molecules to BiF_3, Liu *et al.*[18] successfully regulated the optical birefringence by changing the coordination environment of Bi^{3+}. Yang *et al.*[19] changed the luminescence color from orange to blue by recrystallizing Cs_2InCl_5 in water. Cordero *et al.*[20] investigated the roles of interstitial water in the structural transitions and stability of $FAPbI_3$ and $MaPbI_3$. Therefore, further investigation into the role of water molecules in the modulation of metal halide properties is essential.

Our group has focused on materials explorations of metal halides[21-24]. In our previous work, we reported dozens of metal halides with nonlinear optical effects, photodegradation effects and photoluminescence properties[25,26]. By introducing water, we successfully promoted the generation of more local photoelectrons and increased the photoluminescence quantum yield in metal halides[27]. In this work, a new zero-dimensional alkali-metal tin halide, $K_6Sn_4F_{12}I_2 \cdot 0.5H_2O$, is synthesized by a hydrothermal method. Its structure consists of crystal water molecules and fundamental structural blocks of $[Sn_4F_{12}I_4]$ trapped in $[K_{18}]$ cages. When exposed to air, its color slowly changes from colorless to orange. Experimental measurements combined with theoretical calculations reveal that it is crystal water loss that leads to the color change.

MATERIALS AND METHODS

Synthesis of $K_6Sn_4F_{12}I_2 \cdot 0.5H_2O$

$K_6Sn_4F_{12}I_2 \cdot 0.5H_2O$ single crystals were synthesized by a hydrothermal method at a medium temperature of 493 K. The experimental reagents included NH_4F, KI and $SnCl_2 \cdot 2H_2O$, all of which were of analytical grade from commercial sources and used without further purification. A mixture of 1 g (0.027 mol) of NH_4F, 1 g (0.006 mol) of KI and 1 g (0.004 mol) of $SnCl_2 \cdot 2H_2O$ was placed into the inner liner of a hydrothermal kettle and then 4 mL of deionized water were added. The hydrothermal kettle was sealed and placed in an oven. The mixture was heated to 493 K for 48 h and then cooled to room temperature with a rate of 3 °C/h. After that, colorless transparent $K_6Sn_4F_{12}I_2 \cdot 0.5H_2O$ crystals were obtained.

Single-crystal structure determination

A small $K_6Sn_4F_{12}I_2 \cdot 0.5H_2O$ crystal with dimensions of $0.12 \times 0.10 \times 0.08$ mm^3 was selected for single-crystal structure determination. The diffraction data were collected on a Rigaku AFC10 single-crystal diffractometer equipped with graphite-monochromated Mo Kα radiation (λ = 0.71073 Å) at 293 K. The crystal structures were solved by direct methods with the program SHELXS-97 and refined by full-matrix least squares on F^2 by SHELXTL. The structures were verified using the ADDSYM algorithm from the program PLATON and no higher symmetry was found. The relevant crystallographic data, atomic coordinates, isotropic and anisotropic displacement parameters and selected bond distances and angles are listed in Supplementary Tables 1-4.

Powder X-ray diffraction

Powder X-ray diffraction (XRD) of the polycrystalline samples was performed at room temperature using an automated Bruker D8 Focus X-ray diffractometer equipped with a diffracted monochromator set for Cu Kα (λ = 1.5418 Å) radiation. A scanning step width of 0.02° and a scanning rate of 0.1°s^{-1} were applied to record the patterns in the 2Θ range of 10-70°.

Thermal analysis

Thermogravimetric analysis was performed on an EXSTAR TG/DTG thermogravimetric analyzer. The sample was placed in an alumina crucible, which was heated at a rate of 15 °C/min under N_2 flow from room temperature to 900 °C.

UV transmittance spectroscopy

The UV transmittance spectra of $K_6Sn_4F_{12}I_2$•0.5H_2O before and after the phase transition were collected with a Varian Cary 5000 UV-vis-NIR spectrometer in the wavelength range from 300 to 1400 nm. A $BaSO_4$ plate was used as a standard.

Computational methods

The first-principles calculations for $K_6Sn_4F_{12}I_2$•0.5H_2O were performed using the planewave pseudopotential method implemented in the CASTEP package based on density functional theory. The CA-PZ functionals of local density approximation were adopted to describe the exchange-correlation functionals. The planewave energy cutoff, self-consistent-field tolerance and k-point separation were set as 450 eV, 1.0 × 10^{-6} eV/atom and 0.05 Å^{-1}, respectively. To investigate the role of crystal water molecules in the bandgap, a hypothetical structure $K_6Sn_4F_{12}I_2$ obtained by removing the water molecules of $K_6Sn_4F_{12}I_2$•0.5H_2O was also calculated under the same parameters. Our tests revealed that the above computational parameters are sufficiently accurate for present purposes.

RESULTS AND DISCUSSION

Single crystals of $K_6Sn_4F_{12}I_2$•0.5H_2O were obtained by a hydrothermal method using the raw materials of 1 g (0.027 mol) of NH_4F, 1 g (0.006 mol) of KI and 1 g (0.004 mol) of $SnCl_2$•2H_2O dissolved in 4 mL of deionized water. The mixture was reacted at 493 K and further slowly cooled to room temperature. Colorless transparent crystals of $K_6Sn_4F_{12}I_2$•0.5H_2O were obtained [Figure 1A]. The crystal structure was solved and refined on the basis of single-crystal data. The powder XRD patterns of obtained crystals show good agreement with the calculated results derived from the single-crystal data [Figure 1B], indicating the purity of the obtained samples (crystal data, atomic coordinates, atomic displacement parameters and bond distances and angles are given in Supplementary Tables 1-4).

$K_6Sn_4F_{12}I_2$•0.5H_2O crystallizes in the cubic centrosymmetric space group of Fd-3m (No. 227) with unit cell parameters of a = b = c = 17.1860 Å. All the atoms are occupied in one crystallographically unique position in the symmetric unit. The K, Sn, F, I, O and H ions are at Wyckoff positions *48f*, *32e*, *96g*, *16c*, *8b* and *32e*. In the structure, the Sn^{2+} cations are coordinated with three F$^-$ anions and form [SnF$_3$] triangular pyramids for the presence of stereochemically active lone-pair electrons on Sn^{2+} cations. The Sn-F bonds length are 2.0709 Å and the F-Sn-F angles are 84.156°, both of which are comparable with those in ASnF$_3$ (A = Na, K, Rb or Cs)[28,29], indicating the rationality of our structural solution.

In order to illuminate the structure clearly, the [Sn$_4$F$_{12}$] supertetrahedra, [I$_4$] tetrahedra and [K$_{18}$] cage are displayed in Figure 2A. The [Sn$_4$F$_{12}$] supertetrahedra are composed of four [SnF$_3$] triangular pyramids with the Sn^{2+} cations located at the vertex. Every four isolated I$^-$ anions can construct the [I$_4$] tetrahedra, which are staggered with the [Sn$_4$F$_{12}$] supertetrahedra and formed the cubic [Sn$_4$F$_{12}$I$_4$] fundamental structural
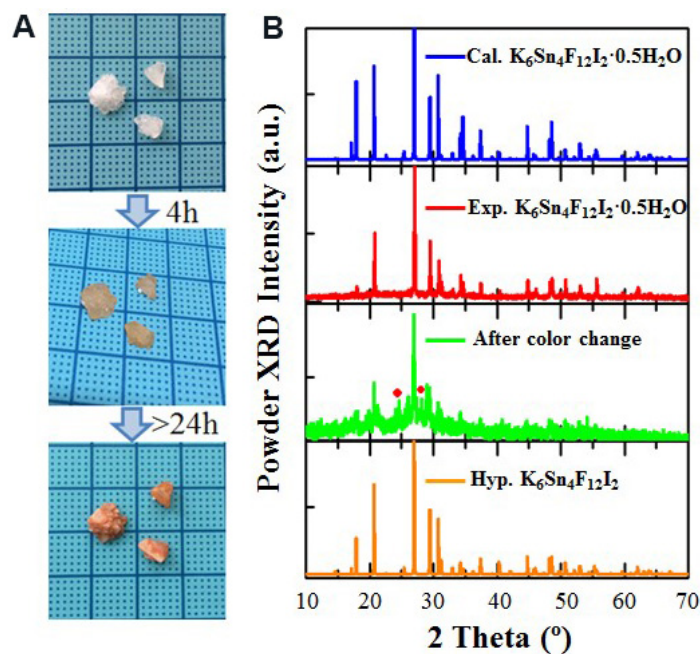
Figure 1. (A) Photographs of obtained single crystals with color change. (B) Powder XRD patterns of $K_6Sn_4F_{12}I_2 \cdot 0.5H_2O$. XRD: X-ray diffraction.
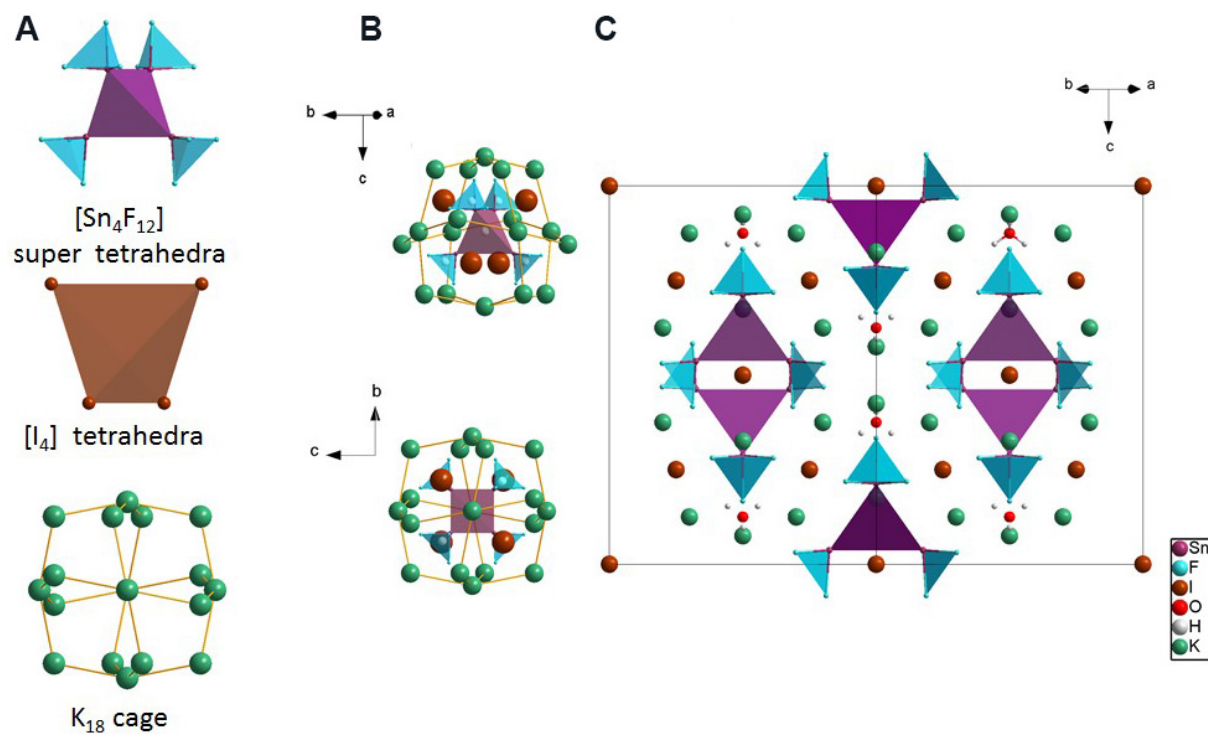
Figure 2. (A) $[Sn_4F_{12}]$ supertetrahedra, $[I_4]$ tetrahedra and $[K_{18}]$ cage. (B) $[Sn_4F_{12}I_4]$ fundamental structural block in $[K_{18}]$ cage. Upper panel, view along the [210] direction, and lower panel, view along the *a*-axis. (C) Structure of $K_6Sn_4F_{12}I_2 \cdot 0.5H_2O$.

blocks. In this cubic $[Sn_4F_{12}I_4]$ fundamental structural block, the $[SnF_3]$ triangular pyramids and I^- anions occupy the eight vertexes, respectively. The K^+ cations are inserted into the space between the $[Sn_4F_{12}I_4]$

fundamental structural blocks and every eighteen K^+ cations construct a $[K_{18}]$ cage, as shown in Figure 2A. These $[K_{18}]$ cages further trap the cubic $[Sn_4F_{12}I_4]$ fundamental structural blocks, as shown in Figure 2B. The distance between the neighboring K^+ cations in the $[K_{18}]$ cages is 4.4637 Å, which is large enough to hold the cubic $[Sn_4F_{12}I_4]$ fundamental structural blocks. All K^+ cations are six-coordinated to F^- anions with two short K-F bonds of 2.7735 Å and four long bonds of 2.8792 Å. The F-K-F angles vary from 57.632° to 123.107°, resulting in a planar arrangement of the four farther F^- anions, which makes the $[KF_6]$ polyhedra adopt a saddle-like shape. These saddle-like polyhedra further construct the three-dimensional framework by sharing the edges, as shown in Supplementary Figure 1. After adding the crystal water molecules, the fundamental structural blocks construct the crystal structure of $K_6Sn_4F_{12}I_2 \cdot 0.5H_2O$ shown in Figure 2C.

As shown in Figure 1A, when exposed to air, $K_6Sn_4F_{12}I_2 \cdot 0.5H_2O$ exhibits a color change from colorless to orange within 24 h. It should be noted that this phenomenon only occurs on the surface, with the internal color unchanged, even after exposure in air for one month. As a result, a single-crystal structure solution is not available for the microscopic structure of the compound after the color change. In order to investigate the color change mechanism, experimental characterization of the powder samples (obtained by grinding the single crystals and exposing them to air for more than 24 h) and theoretical calculations are performed.

The powder XRD patterns of the samples after the color change are shown in Figure 1B. As shown, the patterns are highly consistent with those before the color change, except for the decrease in crystallinity and two peaks from unknown compounds. This means that the color change does not change the powder XRD patterns. UV-vis-NIR diffuse-reflectance spectra for the samples before and after the color change were measured and the results are exhibited in Figure 3A. As the results show, the shortest absorption edges are 350 and 565 nm for $K_6Sn_4F_{12}I_2 \cdot 0.5H_2O$ before and after the color change, corresponding to 3.5 and 2.2 eV, respectively. The results also agree well with the sample colors before (colorless) and after (orange) the change. Thermogravimetric measurements were also carried out to evaluate the stability of $K_6Sn_4F_{12}I_2 \cdot 0.5H_2O$ and the results are shown in Figure 3B. Clearly, $K_6Sn_4F_{12}I_2 \cdot 0.5H_2O$ started losing weight at the beginning and finally remained at ~45% after the thermal measurement. Even close to room temperature, the weight of $K_6Sn_4F_{12}I_2 \cdot 0.5H_2O$ decreased. This means that $K_6Sn_4F_{12}I_2 \cdot 0.5H_2O$ possesses relatively low stability and its color change happens with weight loss at room temperature, which is consistent with the observations from the UV-vis-NIR diffuse-reflectance experiments. Considering the slow weight loss and relatively low transition temperature, $K_6Sn_4F_{12}I_2 \cdot 0.5H_2O$ is most likely to lose crystal water during the color change.

As the crystal structure after the color change is unavailable, first-principles calculations[30] on $K_6Sn_4F_{12}I_2 \cdot 0.5H_2O$ and its anhydrous structure $K_6Sn_4F_{12}I_2$ (hypothetical) were performed to investigate the color change mechanism. The hypothetical structure $K_6Sn_4F_{12}I_2$ was built by removing the crystal water and its structure was optimized. After geometry optimization, the obtained structure of $K_6Sn_4F_{12}I_2$ possesses well-matching powder XRD patterns [Figure 1B] with the experimental ones after the color change, which proves the rationality of our hypothesis. As shown in Figure 4A, the calculated band gap of 2.24 eV for $K_6Sn_4F_{12}I_2 \cdot 0.5H_2O$ is smaller than the experimental value of 3.5 eV, owing to the discontinuity of the exchange-correlation energy[31]. When the crystal water molecules are removed from the structure, $K_6Sn_4F_{12}I_2$ exhibits a smaller band gap of 1.96 eV [Figure 4C]. This trend agrees well with the experimental observations and can be accounted for the color change that the water loss makes the band gap smaller. In addition, we further calculated the partial density of states between the bandgap projected on the constituent elements of $K_6Sn_4F_{12}I_2 \cdot 0.5H_2O$ [Figure 4B] and the hypothetical $K_6Sn_4F_{12}I_2$ [Figure 4D]. Clearly, for both compounds, the electronic states close to band gaps are mainly composed of Sn and I orbitals, indicating that their shortest absorption edges are both determined by the heavy element atoms, i.e., Sn and
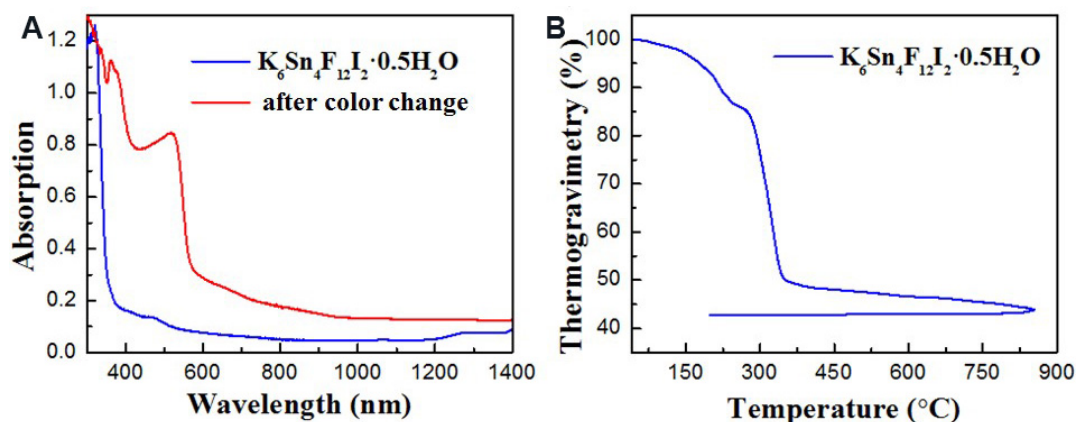
Figure 3. (A) UV-vis-NIR diffuse-reflectance spectra of $K_6Sn_4F_{12}I_2 \cdot 0.5H_2O$ before (blue) and after (red) color change. (B) Thermogravimetric analysis curve of $K_6Sn_4F_{12}I_2 \cdot 0.5H_2O$.
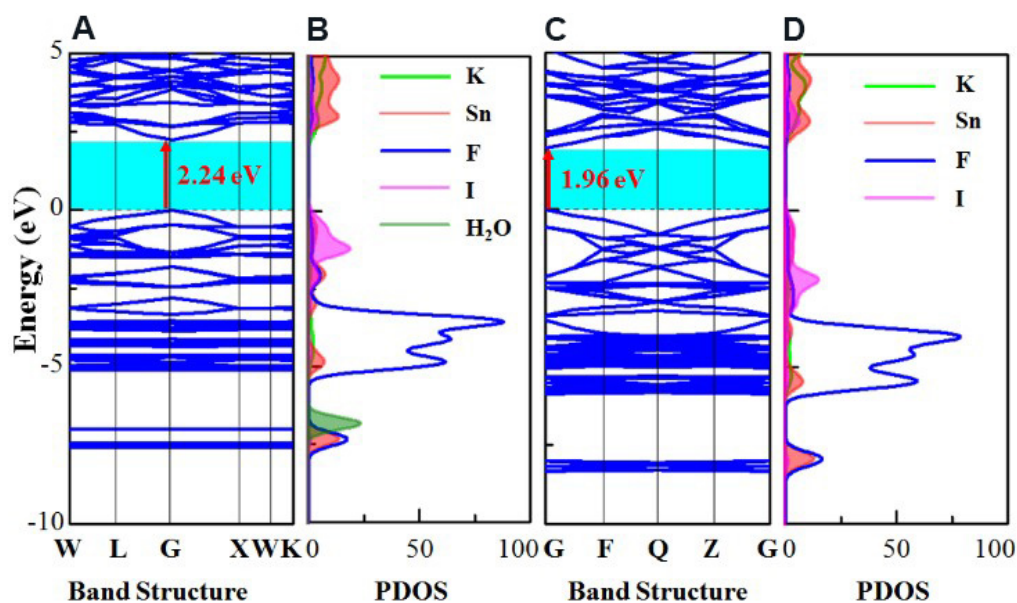
Figure 4. Calculated electronic band structure and PDOS projected on the constituent elements of $K_6Sn_4F_{12}I_2 \cdot 0.5H_2O$ and hypothetical $K_6Sn_4F_{12}I_2$. (A) and (B) for the former and (C) and (D) for the latter. PDOS: Partial density of states.

I. However, the presence of crystal water molecules changes the local coordinating environments of Sn and I, which affect their band structure. As shown, the orbitals of I are more localized at the top of valence bands in $K_6Sn_4F_{12}I_2 \cdot 0.5H_2O$. In comparison, the orbitals of I at the top of valence bands in $K_6Sn_4F_{12}I_2$ are more disperse for the absence of water, which leads to the reduction of the band gap and further results in the color change.

CONCLUSIONS

In summary, a new alkali-metal tin halide, $K_6Sn_4F_{12}I_2 \cdot 0.5H_2O$, was synthesized by a hydrothermal method. It possesses a zero-dimensional structure consisting of crystal water molecules and $[Sn_4F_{12}I_4]$ fundamental structural blocks trapped in $[K_{18}]$ cages. Interestingly, $K_6Sn_4F_{12}I_2 \cdot 0.5H_2O$ exhibits a color change from colorless to orange when exposed to air. Experimental measurements and theoretical calculations were

performed and the results revealed that this color change is attributed to the loss of crystal water in the microstructure.

DECLARATIONS

Acknowledgments

Authors' contributions
Performed the experiments and calculations and wrote the initial draft of the manuscript: Gong P
Conceived the idea: Luo S
Provided the calculation package and analysis tools: Lin Z
All authors contributed to the general discussion.

Availability of data and materials
Crystallographical data (CIF) and additional data in Supplementary Materials. Deposition number CCDC 2104252 for $K_6Sn_4F_{12}I_2 \cdot 0.5H_2O$.

Financial support and sponsorship

Conflicts of interest
All authors declared that there are no conflicts of interest.

Ethical approval and consent to participate
Not applicable.

Consent for publication
Not applicable.

Copyright

REFERENCES

1. Zhang R, Mao X, Yang Y, et al. Air-stable, lead-free zero-dimensional mixed bismuth-antimony perovskite single crystals with ultra-broadband emission. *Angew Chem Int Ed Engl* 2019;58:2725-9. DOI PubMed
2. Zhou L, Liao JF, Huang ZG, et al. A highly red-emissive lead-free indium-based perovskite single crystal for sensitive water detection. *Angew Chem Int Ed Engl* 2019;58:5277-81. DOI PubMed
3. Zhou C, Lin H, Tian Y, et al. Luminescent zero-dimensional organic metal halide hybrids with near-unity quantum efficiency. *Chem Sci* 2018;9:586-93. DOI PubMed PMC
4. Saouma FO, Stoumpos CC, Wong J, Kanatzidis MG, Jang JI. Selective enhancement of optical nonlinearity in two-dimensional organic-inorganic lead iodide perovskites. *Nat Commun* 2017;8:742. DOI PubMed PMC
5. Hao F, Stoumpos CC, Cao DH, Chang RPH, Kanatzidis MG. Lead-free solid-state organic-inorganic halide perovskite solar cells. *Nature Photon* 2014;8:489-94. DOI
6. Xing G, Mathews N, Sun S, et al. Long-range balanced electron- and hole-transport lengths in organic-inorganic $CH_3NH_3PbI_3$. *Science* 2013;342:344-7. DOI PubMed
7. Li L, Shang X, Wang S, et al. Bilayered hybrid perovskite ferroelectric with giant two-photon absorption. *J Am Chem Soc* 2018;140:6806-9. DOI PubMed
8. You YM, Liao WQ, Zhao D, et al. An organic-inorganic perovskite ferroelectric with large piezoelectric response. *Science* 2017;357:306-9. DOI PubMed
9. Connor BA, Leppert L, Smith MD, Neaton JB, Karunadasa HI. Layered halide double perovskites: dimensional reduction of $Cs_2AgBiBr_6$. *J Am Chem Soc* 2018;140:5235-40. DOI PubMed

10.   Chen B, Li T, Dong Q, et al. Large electrostrictive response in lead halide perovskites. *Nat Mater* 2018;17:1020-6. DOI PubMed

11.   Huang L, Wang Q, He F, et al. Synthesis, crystal structures and nonlinear optical properties of polymorphism: α- and β-RbHgI$_3$·H$_2$O. *J Alloys Compd* 2019;771:547-54. DOI

12.   Zhou C, Lin H, Neu J, et al. Green emitting single-crystalline bulk assembly of metal halide clusters with near-unity photoluminescence quantum efficiency. *ACS Energy Lett* 2019;4:1579-83. DOI

13.   Li Z, Li Y, Liang P, Zhou T, Wang L, Xie R. Dual-band luminescent lead-free antimony chloride halides with near-unity photoluminescence quantum efficiency. *Chem Mater* 2019;31:9363-71. DOI

14.   Wu Q, Meng X, Zhong C, Chen X, Qin J. Rb$_2$CdBr$_2$I$_2$: a new IR nonlinear optical material with a large laser damage threshold. *J Am Chem Soc* 2014;136:5683-6. DOI PubMed

15.   Zhang G, Li Y, Jiang K, et al. A new mixed halide, Cs$_2$HgI$_2$Cl$_2$: molecular engineering for a new nonlinear optical material in the infrared region. *J Am Chem Soc* 2012;134:14818-22. DOI PubMed

16.   Zheng X, Liu Y, Liu G, et al. Crystalline mixed halide halobismuthates and their induced second harmonic generation. *Chem Mater* 2016;28:4421-31. DOI

17.   Huang Y, Meng X, Gong P, Lin Z, Chen X, Qin J. A study on K$_2$SbF$_2$Cl$_3$ as a new mid-IR nonlinear optical material: new synthesis and excellent properties. *J Mater Chem C* 2015;3:9588-93. DOI

18.   Liu X, Yang C, Wu Q, Sun J, Liang F. From BiF$_3$ to BiF$_3$·H$_2$O: diverse Bi(iii) coordination for structural transformation and birefringence regulation. *CrystEngComm* 2020;22:6838-46. DOI

19.   Yang C, Guo F, Zhang Y, et al. Luminescence change from orange to blue for zero-dimensional Cs$_2$InCl$_5$(H$_2$O) metal halides in water and a new post-doping method. *Chem Asian J* 2021;16:1619-25. DOI

20.   Cordero F, Craciun F, Paoletti AM, Zanotti G. Structural transitions and stability of FAPbI$_3$ and MAPbI$_3$: the role of interstitial water. *Nanomaterials (Basel)* 2021;11:1610. DOI PubMed PMC

21.   Gong P, Luo S, Huang Q, et al. An alkaline tin(II) halide compound Na$_3$Sn$_2$F$_6$Cl: synthesis, structure, and characterization. *J Solid State Chem* 2017;248:104-8. DOI

22.   Gong P, Luo S, Xiao K, et al. Structure and characterization of a zero-dimensional alkali tin dihalides compound Cs$_3$Sn$_3$F$_2$Cl$_7$ with the [Sn$_2$F$_2$Cl$_4$]$^{2-}$ clusters. *Inorg Chem* 2017;56:3081-6. DOI PubMed

23.   Gong P, Yang Y, You F, et al. A SbF$_3$Cl (A = Rb, Cs): structural evolution from centrosymmetry to noncentrosymmetry. *Cryst Growth Des* 2019;19:1874-9. DOI

24.   Song G, Li M, Yang Y, et al. Lead-free tin(IV)-based organic-inorganic metal halide hybrids with excellent stability and blue-broadband emission. *J Phys Chem Lett* 2020;11:1808-13. DOI PubMed

25.   Gong P, Luo S, Yang Y, et al. Nonlinear optical crystal Rb$_4$Sn$_3$Cl$_2$Br$_8$: synthesis, structure, and characterization. *Cryst Growth Des* 2018;18:380-5. DOI

26.   Song G, Li Z, Gong P, Xie R, Lin Z. Tunable white light emission in a zero-dimensional organic-inorganic metal halide hybrid with ultra-high color rendering index. *Adv Optical Mater* 2021;9:2002246. DOI

27.   Song G, Li M, Zhang S, et al. Enhancing photoluminescence quantum yield in 0D metal halides by introducing water molecules. *Adv Funct Mater* 2020;30:2002468. DOI

28.   Salami TO, Zavalij PY, Oliver SR. Synthesis and crystal structure of two tin fluoride materials: NaSnF3 (BING-12) and Sn3F3PO4. *J Solid State Chem* 2004;177:800-5. DOI

29.   Zemnukhova LA, Fedorishcheva GA. Study of isomorphism in fluorine-containing antimony(III) complexes. *Russ Chem Bull* 1999;48:104-9. DOI

30.   Clark SJ, Segall MD, Pickard CJ, et al. First principles methods using CASTEP. *Z Kristallogr Cryst Mater* 2005;220:567-70. DOI

31.   Wang CS, Klein BM. First-principles electronic structure of Si, Ge, GaP, GaAs, ZnS, and ZnSe. II. Optical properties. *Phys Rev B* 1981;24:3417-29. DOI